ACS Photonics

Article

pubs.acs.org/journal/apchd5

Plasmonic–Photonic Mode Coupling in Indium-Tin-Oxide Nanorod Arrays

Shi-Qiang Li,[†] Peijun Guo,[†] D. Bruce Buchholz,[†] Wei Zhou,[†] Yi Hua,[†] Teri W. Odom,[†,‡,§] J. B. Ketterson,[§,⊥] Leonidas E. Ocola,[∥] Kazuaki Sakoda,[§,#] and Robert P. H. Chang*[,†,§]

[†]Department of Materials Science and Engineering, Northwestern University, 2220 Campus Drive, Evanston, Illinois 60208-3108, United States

[‡]Department of Chemistry, Northwestern University, 2145 Sheridan Road, Evanston, Illinois 60208-3113, United States

[§]NU-NIMS Materials Innovation Center, 2220 Campus Drive, Evanston, Illinois 60208-3108, United States

[⊥]Department of Physics, Northwestern University, 2145 Sheridan Road, Evanston, Illinois 60208-3113, United States

[∥]Center for Nanoscale Materials, Argonne National Laboratory, Lemont, Illinois 60439, United States

[#]National Institute for Materials Science, 1-2-1 Sengen, Tsukuba, Ibaraki 305-0047, Japan

Supporting Information

ABSTRACT: We present a systematic study of light scattering from indium-tin-oxide (ITO) nanorods in the near-infrared with a special focus on the resonant coupling of plasmonic transverse mode and photonic modes in 2-D periodic arrays. Using theoretical analysis combined with simulations, a set of experiments has been designed to study such interactions. Near-field mapping from the simulations shows a strong interaction of localized surface plasmon resonances (LSPR) with a photonic resonance; together they explain the scattering phenomenon observed in our experiments carried out in the far field. We observed the shift of LSPR as the plasma frequency was varied, resulting in a modification of the spectral shape. Utilizing the high aspect ratios of the ITO nanorods, the LSPR strength can be turned on and off by the polarization of the incident light.

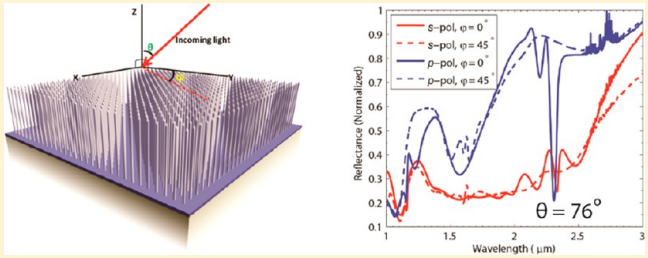

KEYWORDS: *degenerated semiconductor, optically induced transparency, transparent conducting oxide, nanophotonics, Bragg resonance, plasmonic crystal*

Research in the manipulation of light at the nanoscale has expanded rapidly in the past decade as a result of new instruments for nanofabrication and characterization. In addition, with easier access to high-performance computing, design and modeling are now routinely carried out prior to experimentation. These capabilities have accelerated proof-of-principle demonstrations of many prototype devices involving optical computing,[1,2] surface-enhanced Raman spectroscopy,[3] nanolasers,[4,5] and optical circuits.[6−8] The interaction of light with 2-D plasmonic particle arrays is a topic under intensive study due to the rich physics underlying such interactions.[9−18] Most work on nanostructured arrays is about planar structures, i.e., structures with a relatively small extension in the third dimension.[19−22] Although the study on 2-D dielectric photonic crystal slabs has been extensive,[23−26] the study of plasmonic nanostructure arrays with a high aspect ratios has been mostly limited to pseudo-2-D arrays with long axis lying in-plane.[14,20,27] There are some examples of 2-D nanorod arrays (NRAs) of silver and gold with a high aspect ratio (grown by filling anodized aluminum oxide (AAO) patterned holes); however, they have limited applicability to creating periodic arrays with designed lattices and spacings.[28−32] Recently we reported a versatile method of fabricating indium-tin-oxide (ITO) NRAs using a vapor–liquid–solid technique and demonstrated the presence of both isolated and collective plasmon modes.[33] These nanostructures are both mechanically and chemically stable in air, making them easy to use in our experiments. Indium-tin-oxide nanorods (ITO-NRs) possess many unique features: (1) They have good electrical properties due to their single-crystalline quality; (2) the rod length can be controlled by the growth time; (3) the array can be defined through the position and size of the gold catalytic nanoparticles used in our synthesis; (4) the intrinsic plasma frequency of the ITO-NRs is tunable via a postgrowth annealing; (5) the Drude model can be used to calculate the permittivity $\varepsilon(\lambda)$ (in the spectral regime under study, it is free of other Lorentzian poles). For our ITO-NRs, the real part of permittivity becomes negative in the near-infrared (NIR), a requirement for the existence of plasmons.

Received: September 15, 2013
Published: February 13, 2014

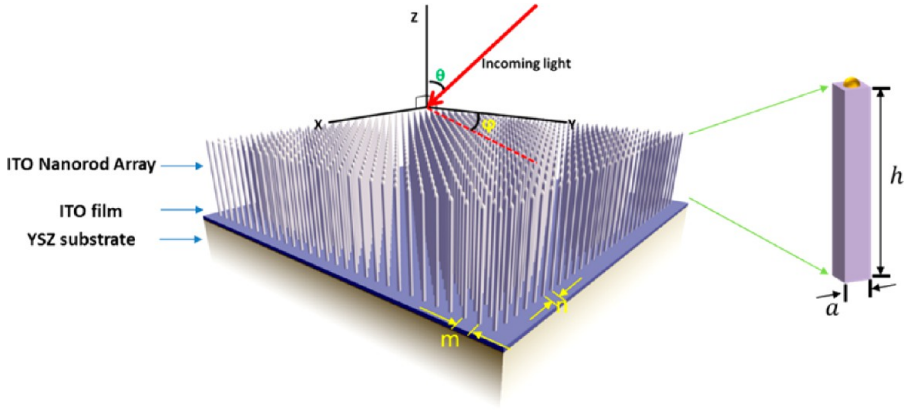

Figure 1. Schematic diagram of a typical ITO nanorod array.

In general, resonances, coupling among modes, and wave−particle interactions are of great interest in science. Unlike gold and silver, ITO-NRAs are unusual in that they show strong resonant responses in the NIR regime. In such a system we can independently vary the height of the ITO-NRs, their lattice structure, lattice parameters, and the plasma frequency. This provides us with a rich phase space where scattering and mode-coupling phenomena can be studied systematically. For example, by selecting a combination of the above parameters, localized (or propagating) plasmon modes, photonic modes, or fundamental and higher-order plasmon modes[34] can be excited along with the coupling among these modes. In this article, we focus on the coupling of photonic and localized plasmon modes by using simulations to guide the experiments. In this way we can be assured that other potential modes of the system are minimized in the spectral region studied (1 to 3 μm in wavelength).

This article is organized as follows: First, we discuss the scattering behavior of an isolated nanorod based on the scattering theory, followed by numerical simulations using the discrete dipole approximation (DDA) and the finite-element method (FEM). From the simulations, the scattering of the ITO-NR in a periodical array is compared with that of an isolated nanorod. We intentionally set the periodicity and the incident light angle so the photonic modes will be in the vicinity of the localized plasmon resonances, allowing us to study the interaction of these modes. We then discuss the various spectral features in our experiments. Finally we present a summary of the research.

THEORETICAL BACKGROUND, SIMULATION, AND EXPERIMENTS

Scattering Theory of Isolated Nanorod. We start with a brief discussion of how light interacts with an isolated nanostructure and then consider an array of such structures. For simple isolated metallic structures like spheres, infinite cylinders, and spheroids, the scattering properties can be described analytically using the Mie theory.[35] In the limit of very small structures, the electrostatic Rayleigh−Gans theory applies.[36]

When light with wavelength λ is scattered from a metallic sphere with radius much smaller than λ, according to Mie scattering theory, a resonant peak occurs when $\varepsilon' = -2\varepsilon_d$, where ε' is the real part of the dielectric of the metal and ε_d is that of the surrounding. This condition is termed local surface plasmon resonance (LSPR), which occurs as a result of collective electron motion on the surface of a metallic sphere in resonance with the light. The resonance peak is unique, independent of polarization and direction of the incident light, owing to the spherical geometry. For an anisotropic structure such as a cylindrical rod, the electron oscillation along the axial direction (longitudinal mode) experiences a lower restoring force, resulting in a longer resonant wavelength, while the short axis (transverse mode) has the opposite behavior. As the aspect ratio of the cylindrical rod increases (approaching infinity), the resonance conditions for the transverse mode approach asymptotically the condition $\varepsilon' = -\varepsilon_d$, while the resonance for the longitudinal mode disappears.[37] (More details are provided in the Supporting Information (SI).)

The Case of ITO-NRs. It is now well known that LSPR is sensitive to the details of the particle geometry. The behavior of ITO-NRs is similar to a cylindrical rod discussed above. However, the base of our ITO-NRs is close to a square, so the transverse modes will split into multiple modes. In order to simulate or calculate the transverse mode, we need to know $\varepsilon(\lambda)$. In the Drude model,[37] the permittivity of ITO can be described as

$$\varepsilon_{ITO} = \varepsilon_\infty - \frac{{\omega_p}^2}{\left(\frac{hc}{\lambda}\right)^2 + i\gamma\left(\frac{hc}{\lambda}\right)} \quad (1)$$

where ε_∞ is the high-frequency dielectric constant, ω_p is the plasma frequency, h is Planck's constant, c is the speed of light, and λ is the wavelength of light in free space. In the numerical simulations, we chose $\varepsilon_\infty = 3.95$, $\omega_p = 1.36$ eV, and $\gamma = 0.05$ eV.[38] On the basis of the discussion of an infinite cylinder above and eq 1, it can be estimated that the transverse mode of ITO-NR should appear at around 2 μm, at which $\varepsilon_{ITO} = -1$, assuming the surrounding medium is air and a high aspect ratio (usually above 20) of the ITO-NR.

Numerical Simulation. We start this section by defining the geometry used in our simulations and experiments. Figure 1 shows a schematic diagram (not drawn to scale) of the ITO-NRA system studied. The shape of a single nanorod, shown to the right, is represented as a rectangular prism with height h and basal plane dimension a. The ITO-NRs are grown vertically from an ITO film on the substrate, which is (100) yttria-stabilized zirconia (YSZ).

The aligned nanorods are arranged into a rectangular lattice, with the spacing along the x- and y-axis denoted as m and n, respectively. The wave-vector of the incident light is specified

dx.doi.org/10.1021/ph400038g | ACS Photonics 2014, 1, 163−172

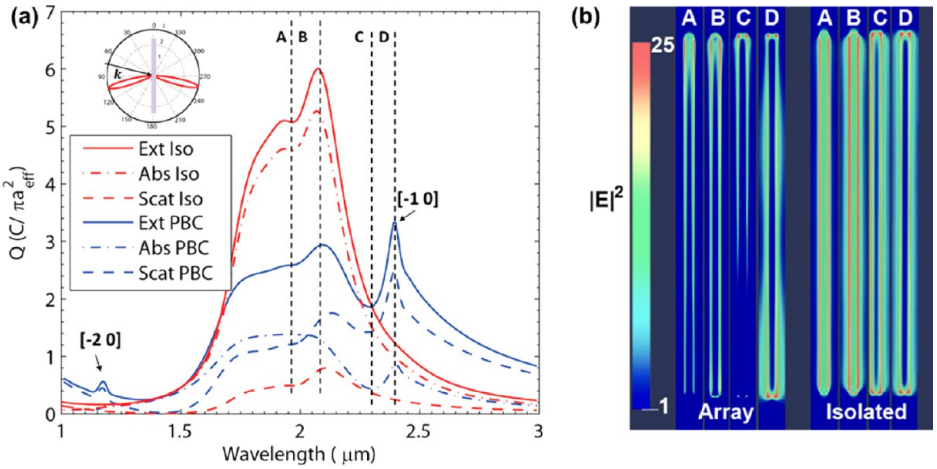

Figure 2. (a) Extinction/scattering/absorption efficiencies of both an isolated ITO nanorod (denoted as Iso in the figure) and a nanorod array generated using periodic boundary conditions (PBC) simulated with s-polarized light. In the inset, a polar plot shows the angular distribution of the scattering efficiency described in the text. The nanorod is represented as a purple rectangle. The positions of photonic modes [−1 0] and [−2 0] are indicated on the curve. (b) Near-field plots for both isolated nanorods and an ITO nanorod in the array at the four typical wavelengths A−D. The geometrical cross-section chosen is the $x-z$ cut plane at the surface of the nanorod facing the incident light (see Figure 1).

by a polar angle φ, measured from the y-axis, and an azimuthal angle θ, measured from z-axis.

We start by simulating an isolated ITO-NR. DDA was used to calculate the transverse modes of an isolated ITO-NR. Developed by Draine and Flatau,[39,40] this method applies to both isolated and periodic targets.[13] The method discretizes an arbitrarily shaped object with equally and closely spaced dipoles. The extinction/scattering/absorption efficiencies (denoted by Q) from DDA simulation, defined as the ratio of the calculated cross sections to the effective geometrical cross-section (πa_{eff}^2), are used to compare the scattering from objects with different shapes. The effective radius a_{eff} of an ITO-NR is defined by the following equation:

$$\frac{4}{3}\pi a_{\mathrm{eff}}^3 = a^2 h$$

where a^2h is the volume of the nanorod. In our simulation, a = 150 nm and h = 5 μm, so a_{eff} = 0.265 μm and the aspect ratio is 33. We simulated the spectrum from 1 to 3 μm at a polar angle θ of 76°, as this is the maximum angle allowed by the experimental setup and a high polar angle is required to obtain strong photonic resonances. It is worth clarifying here that the effective cross-section defined in this paper is not a universal term, as it contains no information of incident angle, which is fixed for our experiments.

The DDA results for both isolated and periodic ITO-NRA are shown in Figure 2. As can be seen, the extinction of an isolated ITO-NR shows two closely spaced peaks around 2 μm, which is characteristic of transverse LSPRs involving more than one mode as a result of the square basal plane. The extinction is dominated by absorption with only very small scattering, since a ranges from 100 to 200 nm, which is much smaller than the wavelength (which is greater than1 μm). The inset on the top-left side of Figure 2a is a polar plot showing the angular distribution of the scattered light at the peak extinction wavelength. The plotted scattering plane is defined by the incident $\vec{k}$ vector and the rod axis (the rod is at the center of the plot). As can be seen, the scattering is mainly in the forward direction and at the angle associated with specular reflection from the rod surface.

For the arrays we first investigate a square lattice with $m = n$ = 1.2 μm. Due to the presence of equal lattice spacings, we expect to have degenerate photonic resonance features. This lattice spacing was chosen so that the lowest order [−1 0] photonic mode lies in the vicinity of the ITO-NR LSPR at approximately 2 μm.

Although in actual experiments a support (substrate) is required for the array, we start by simulating a free-standing (i.e., no substrate) 2-D rod array; we find this captures most of the features occurring in the presence of a support. Such calculations were performed with θ = 76° and φ = 0°, the same angles used for the isolated nanorod calculations. The result is shown as the blue curves in Figure 2a. Compared with the isolated nanorod case, the main plasmon extinction feature has decreased to about half the intensity, and the scattering becomes more prominent than the absorption. Besides this main feature, there is a strong asymmetry at the longer wavelength edge, a sharp dip followed by an abrupt increase at even longer wavelengths. These features are quite similar to those observed by Christ et al.,[41] which were attributed to waveguide excitation of a surface plasmon polariton; such a waveguide layer is not present in our simulation.

The near-field distribution was mapped for the four representative wavelengths, shown in Figure 2b, A−D; these lie near the extinction peak of the isolated rod and at the two extremes of the oscillations for a rod in the array. The plane chosen was the surface of the nanorod facing the incident light.

For isolated rods, the field is localized and uniformly distributed along its length with peaks at the corners; for C and D it is confined to the exterior. Plot B, corresponding to the maximum of the extinction curve, is in good agreement with an LSPR peak. At a longer wavelength, shown in plot C, the enhancement decreases and is only large near the corners.

For a rod in the array, the field tends to be asymmetric along the rod axis; it is also largely exterior to the rod. The field is most uniform in plot B. At the dip of oscillation, shown in C, the field decreases and is largest near the top of the rod. However, at the peak of oscillation, shown in D, the field rises and is concentrated near the bottom.

Considering the geometric arrangement and the permittivity of the ITO-NRAs, two possible light-scattering processes may

dx.doi.org/10.1021/ph400038g | ACS Photonics 2014, 1, 163−172

be involved. First, the transverse LSPR is the only feature exhibited by the isolated nanorod; it also shows up at the same wavelength in the arrays. Due to the fact that the field of LSPR decays rapidly away from the surface,[42] the electric field is tightly confined around the rod. Thus, an LSPR interaction among the nanorods in the array should be minimal, in agreement with the fact that the extinction peak is at the same wavelength in both the isolated rod and the array. Second, the nanorods act as a periodic geometrical grating, resulting in a [−1 0] Bragg resonance at about twice the lattice spacing, 2.4 μm, which is the likely origin of the strong feature that occurs in the vicinity of that wavelength with a sharp Lorentzian-like extinction peak. However, unlike a pure Bragg mode, for which the field should be minimum at the node position (in this case, near a nanorod), the field in this case is strongly enhanced at the surface of the nanorods while being modulated. This implies a coupling between the LSRP mode (located at ~2 μm with a broad line width) and the [−1 0] Bragg resonance (at ~2.4 μm with a sharp line width). Additionally, it creates a locally low absorption peak inside the highly absorptive LSPR peak between position B and D in Figure 2a, analogous to optically induced transparency.[10,43,44]This point will be discussed in more detail later.

We now consider rectangular nanorod arrays. The lattice spacing m = 1.2 μm was retained so that the expected [−1 0] Bragg resonance defined by this lattice spacing remains at the same wavelength as for the square lattice discussed above. On the basis of DDA simulations, the other lattice parameter n was set at 3.15 μm, so as to have the [−1 1] photonic resonances lie within the broad LSPR region. In these simulations, the incident light wave vector is the same as for the square lattice, with $\varphi = 0°$ and $\theta = 76°$. The parameters for the individual rods were the same as for the isolated nanorod and for a rod in the square lattice. Note that in the case of a rectangular lattice the spectral responses at $\varphi = 0°$ and $\varphi = 90°$ differ so that we need to specify whether the wave vector is along the x-axis or y-axis

The extinction/absorption/scattering efficiencies of the ITO-NRA with m = 1.2 μm and n = 3.15 μm are plotted as shown in Figure 3. Results for both s- and p-polarized light are plotted. As the incident wave is nearly perpendicular to the rod axis, the p-polarized wave will have only a small E-field component in the x−y plane; note this is the component that excites the transverse LSPR. On the other hand the s-polarized wave always has an E-field component in the x−y plane, so excitation of the transverse LSPR mode should be large. As expected, the extinction curve (shown as the solid curve in Figure 3a) of the s-polarized wave shows a broad extinction feature (i.e., the transverse LSPR), while that for the p-polarized wave (shown as the solid blue curve) has none. Comparing the extinction curve of the s-polarized wave with that of the square lattice shown in Figure 2a, we can see that both of them have a sharp resonance at around 2.4 μm (marked as D in Figure 2b and A in Figure 3); however the rectangular lattice has an additional feature at around 1.7 μm (marked as B in Figure 3), which is distinct from the main peak at 2.1 μm (marked as C in Figure 3). From the set of curves in Figure 3a, it is clear that the main contribution to the features B and C in the extinction curve is from absorption. Contrary to the s-polarization case, the peaks A and C are blue-shifted with p-polarized light and the extinction is mainly due to scattering. Furthermore, the broader feature at B disappears, which is reasonable since only the E-field component in the x−y plane excites transverse LSPRs.

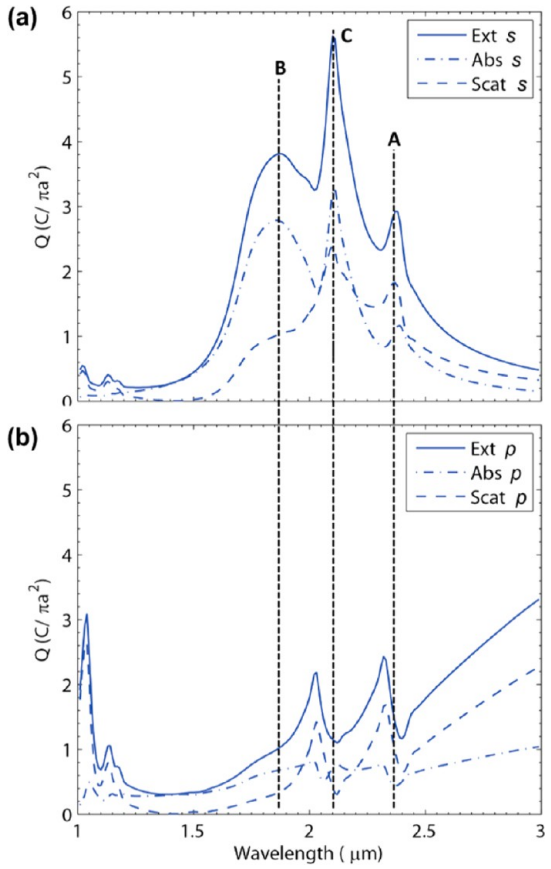

Figure 3. Extinction/absorption/scattering efficiencies of NRA with m = 1.2 μm, n = 3.15 μm. (a) s-Polarized plots and (b) p-polarized plots.

Experimental Verification of the Simulation Results. We fabricated the ITO-NRAs according to the parameters chosen in DDA simulations and show that the DDA simulations can accurately predict the various resonance properties observed in the experiments.

To fabricate vertically aligned ITO-NRA with a prescribed lattice spacing, the choice of substrate and the patterning techniques are crucial. The processing steps employed are shown in Figure 4a. Single-crystal YSZ (100) (from MTI Corp.) was used for the substrate. It has an excellent lattice match with the ITO, leading to aligned growth of ITO single-crystal nanorods.[45] Due to the surface energy effect of the YSZ found in our experiments, it is necessary to deposit a thin film of ITO to prevent the nanorods from growing laterally rather than vertically. In our experiments, pulsed laser deposition was used to grow an epitaxial film of ITO on a (100) YSZ substrate, as shown in step 1 of Figure 4a.

A patterned gold catalyst array is used for VLS nanorod growth. A large array (>0.25 cm^2) is required for angle-resolved optical measurements. In order to make these patterns repetitively and efficiently, soft interference lithography[46] was adopted to fabricate a shadow mask from a silicon master made by e-beam lithography (with a Joel JBL-9300 system and HSQ as photoresist), so that different patterns can be designed for repetitive use. The features in these patterns are round holes 100 nm in diameter. The shadow mask was then transferred to the ITO/YSZ substrate shown as step 2 in Figure 4a. Once the mask was in place, e-beam evaporation was performed to deposit 1.5 nm Cr followed by 20 nm Au. Then lift-off was performed to remove the shadow mask (steps 3 and 4 in Figure

dx.doi.org/10.1021/ph400038g | ACS Photonics 2014, 1, 163−172

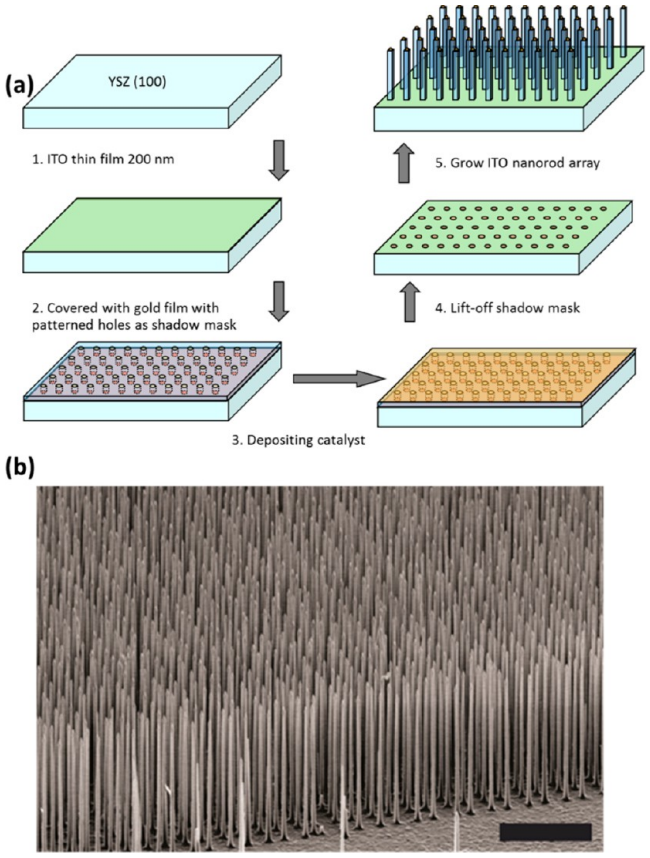

Figure 4. (a) The steps used to fabricate ITO-NRAs. (b) SEM image of vertically aligned ITO-NRA fabricated according to the steps in panel a; the tilt angle with respect to surface normal is 65°. The lattice spacings m and n are 1.8 and 2.2 μm, respectively. The scale bar is 10 μm.

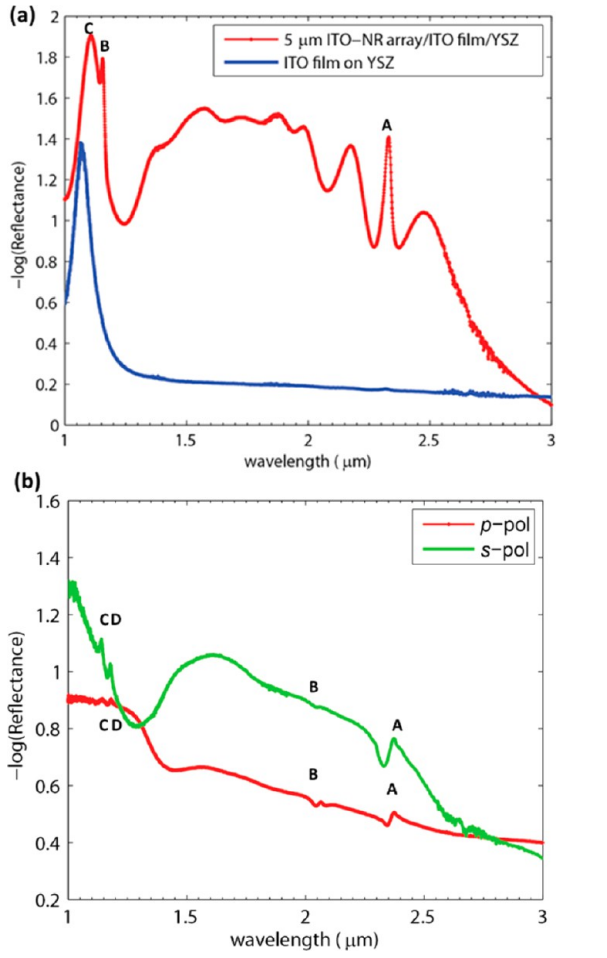

Figure 5. (a) Spectrum of an ITO-NRA with 5 μm height in a square lattice (lattice constant is 1.2 μm) plotted together with the spectrum of an ITO film on a YSZ substrate. (b) Reflectance curves of NRA with rectangular lattice, with m = 1.2 μm and n = 3.15 μm. Measurements were performed with polarized light.

4a). Following that, the sample was heated in a furnace for NRA growth, with indium and stannous oxide (mixed with atomic ratio 9:1) as a precursor located upstream.[33] The subsequently formed structure is shown as step 5 of Figure 4a, and an SEM image of a fabricated NRA is shown in Figure 4b. The sample was tilted by 65° with respect to the beam axis to reveal the vertical dimension. It can be seen that the nanorods are quite uniform in terms of height and diameter and that they are well positioned at lattice sites with only small displacements.

Optical measurements including specular reflection and zero-order transmission were performed with a Bruker Vertex 70 setup with a near-infrared light source and an extended range KBr beam splitter; in addition we fabricated a stage to vary the sample orientation. The light was polarized with a ZnSe infrared ruled wire grid polarizer (from Edmund Optics). The incident θ angle was fixed at 76° throughout the experiment.

A square ITO-NRA (with $m = n = 1.2$ μm) was fabricated, and the transmittance and reflectance spectra were measured. A gold mirror with a 200 nm gold coating was used as a 100% reflectance reference. Due to the presence of the ITO film used for the fabrication process and the YSZ substrate, as well as the high reflectance from the air/YSZ substrate interface when the incident angle θ is large, most of the light is reflected and negligible transmittance was measured. In order to compare with the extinction efficiency shown in Figure 2a, $-\log_{10}$(reflectance) is shown as the red curve in Figure 5a.

The sharp feature A at around 2.3 μm corresponds to the [−1 0] mode shown in Figure 2a; however, the oscillation is richer than predicted, and the second-order peak B at 1.2 μm is also in good agreement with the position shown in Figure 2. There is a broad hump ranging from 1.3 to 2.5 μm, which is interpreted as the transverse LSPR. This feature is broader than what is predicted by DDA simulation. There is an additional peak at around 1.1 μm marked as C in the plot; we attribute this peak to the ITO film on the YSZ substrate, as can be seen from the blue curve in Figure 5a for the case when only an ITO film is present on the YSZ substrate. The broadening of the LSPR and the richness of oscillations arise from an enhanced interaction of light with the structure as a result of reflection from the substrate; this conclusion is supported by FEM simulations to be discussed in the next section.

Following the same procedure, a NRA with a rectangular lattice was fabricated, and the reflectance spectra are presented in Figure 5b. The reflectance spectrum measured with s-polarized light is plotted as the green curve in Figure 5b; note the large hump from 1.3 to 2.5 μm arising from the LSPR. This feature is suppressed in the p-polarized spectrum due to the very small in-plane electric field component. The [−1 0] photonic peaks are obvious in both curves and marked as A in Figure 5b. The [−1 1] photonic peaks at around 2.0 μm are

dx.doi.org/10.1021/ph400038g | ACS Photonics 2014, 1, 163−172

marked as B. The position of this peak is in good agreement with the feature shown in Figure 3. The higher-order peaks marked as C and D also agree well with the simulations.

Defects, such as missing and displaced nanorods, can occupy as much as 10% of the sample, whereas the simulations assume a perfect rectangular lattice. For the s-polarized reflectance curve, we see that feature B is quite small relative to feature A. Hence we concluded that the $[-1\ 1]$ photonic resonance is more sensitive to defects than the $[-1\ 0]$ photonic resonance.

Effect of Underlying Film and Substrates. In this section, we discuss the behavior of ITO-NRAs in the presence of the underlying ITO film and YSZ substrate, to explain some of the discrepancy between the experimental data and the free-standing NRA simulations.

Guided by the free-standing NRA simulations, together with the experimental data, the simulation box can be chosen more efficiently when performing the more time-consuming simulations, which include the underlying ITO layer and substrate. FEM (COMSOL Multiphysics, RF module) was selected since it has been proven to be more efficient than the DDA when the substrate and underlying film are included. A total-field-scattered-field (TFSF) method was implemented in this paper, which is different from the full-field calculation in our earlier work.[33] A detailed explanation of our simulation setup is included in the SI (Figure S1).

We first simulated a square-lattice ITO-NRA on a YSZ substrate with and without the ITO film together with a free-standing 2-D ITO-NRA, in order to understand the effect of each layer. Figure 6a shows the experimental reflection spectra of the array with and without an ITO layer on the YSZ substrate; Figure 6b shows the corresponding FEM simulations. The polarizer used in this experiment has an extinction ratio above 50:1 for wavelengths above 1.5 μm, but it has limited polarizability below 1.5 μm; thus the experimental reflectance curves are only partially polarized for wavelengths below 1.5 μm. This could cause some deviation from our simulations. The simulations show that the free-standing array has nearly zero reflection, whereas the ITO-NRA in the presence of the substrate has nearly zero transmission due to the strong signal attenuation by the scattering and absorption together with the reflection from the substrate (results are shown in Figure S2 in the SI). In addition, the absorptions of ITO-NRA with and without the ITO film have comparable amplitudes and the same features. As a result, the key features of the coupling of the LSPR modes and the photonic modes can still be addressed with the introduction of the film and substrate, which is the case in these experiments. Note that the superposition of the reflected wave due to the substrate and the incident wave causes a standing wave field distribution, which is significantly different from that of a free-standing ITO-NRA only. This is also shown in the FEM near-field plots. The main features we are addressing here have little change in the presence of the ITO film, as long as the YSZ substrate is there, as shown in Figure 6a,b, which implies that the participation of a grating coupled surface-plasmon polariton (which is a propagating surface plasmon mode) in the ITO film is minimal.

To analyze the interaction of the LSPR mode and photonic resonance, FEM simulations were performed to study the reflectance and absorption spectrum, as well as the near-field distributions. Figure 7a shows the absorption due to the nanorods with different heights, under s-polarized light. The broad absorption peak is due to the LSPR as discussed above, and the sharp dip at around 2.3 μm in the absorption spectrum,

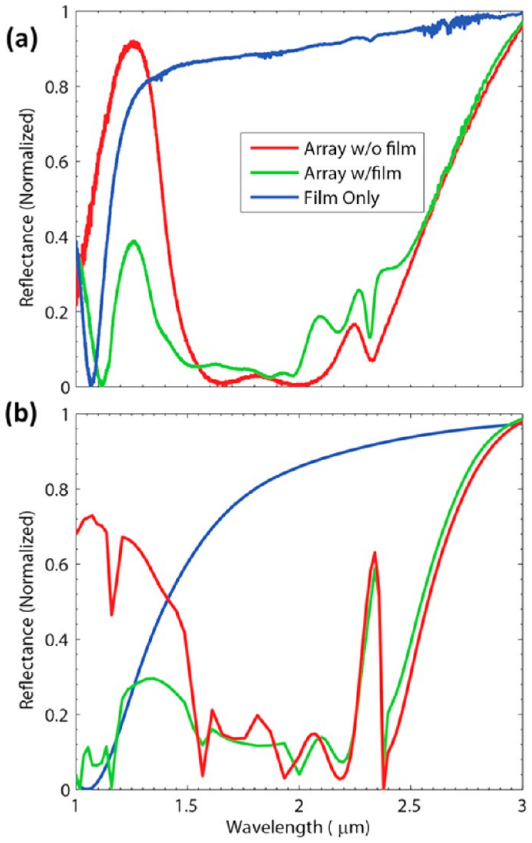

Figure 6. (a) Experimental results on the reflectance from an ITO-NRA on a YSZ substrate. The incident light is s-polarized for all plots. ITO-NRA with an ITO film underneath is the yellow-green curve. The red curve is the spectrum with the thin film etched off. The blue curve is from the ITO film on a YSZ substrate without NRA. (b) The corresponding simulation results obtained with the FEM.

corresponding to the sharp peaks in the reflection spectrum, is due to the coupling of the LSPR resonance and the $[-1\ 0]$ photonic resonance. Point A is the $[-2\ 0]$ photonic mode at around 1.2 μm, which matches with the spacing of the nanorods. At the LSPR resonance, away from the photonic dip (point B), surface enhancement arising from the LSPR is dominant. However, as one approaches the photonic resonance wavelength, instead of being enhanced around each rod, the field is more confined to the space between the rods, and the surface enhancement together with the absorption due to the nanorod decreases (point C). As one moves to the longer wavelength side of the photonic resonance, the near-field profile shows a standing-wave-like field distribution as a result of the superposition of the reflected and incident waves together with the surface enhancement effect due to LSPR (point D and point E). We also note that in the vicinity of the coupling region of the LSPR and the photonic mode, a near-field modulation occurs along both the longitudinal direction (along the rod axis) and the horizontal direction within the plane defined by the incident light and the substrate normal. This is clearly shown by the near-field distribution at point A. Due to the smaller in-plane electric field component, the coupling of the LSPR and photonic mode for p-polarization, shown in Figure 7d, is much smaller than for s-polarization; hence we observe a weaker absorption dip around 2.3 μm and much lower surface field enhancement, as expected.

dx.doi.org/10.1021/ph400038g | ACS Photonics 2014, 1, 163−172

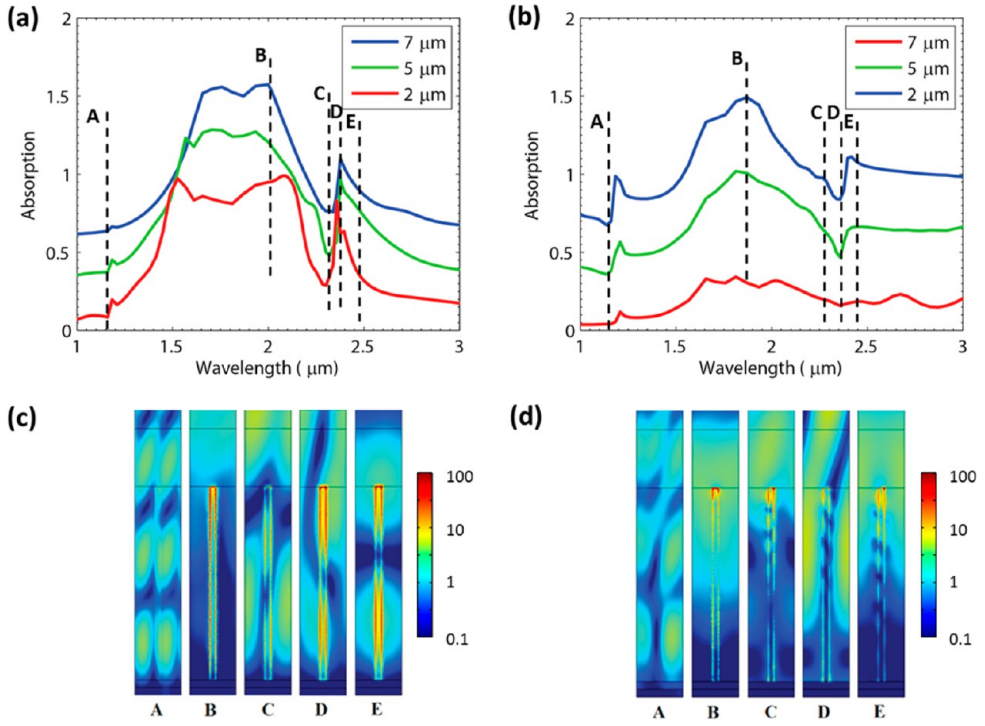

Figure 7. (a and b) Absorption curves of NRAs for three different heights, with an s wave in (a) and p wave in (b), respectively. Absorption is normalized to incident light intensity. Curves are translated along the *y*-axis by 0.3 unit with increasing height for presentation purpose only. (c and d) Near-field maps of a single repetitive unit cell at the *x*−*z* cut plane across the nanorod surface facing the incident light; the height of the nanorod is 5 μm, and the other parameters are the same as DDA simulation. A to E correspond to the spectral positions indicated in the absorption curves in (a) and (b). The scale bars in (c) and (d) are electric field intensities.

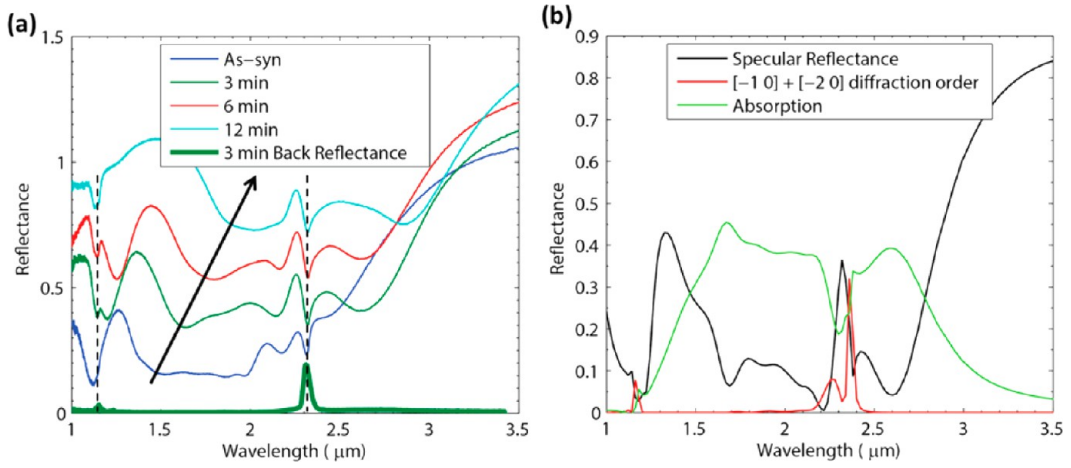

Figure 8. (a) Specular reflectance spectra (θ = 76° and φ = 0°) of 5 μm tall square lattice ITO-NRA. s-Polarized light was used for all measurements. The sample was annealed in dry air in atmospheric pressure at 475 °C. The blue curve is as-synthesized sample; green, red, and cyan curves are 3, 6, and 12 min annealing, respectively. The curves are offset by 20% from each other. The thick black arrowed line traces the red shift of the LSPR with annealing. The backscattering intensity has also been measured for the sample with 3 min annealing and was plotted with a thick line in green without any offset added to distinguish it from other curves. (b) FEM simulation result of specular reflectance, absorption, and the intensity summation of [−1 0] and [−2 0] diffraction orders. All of the curves are normalized to total incident intensity.

Tunable Plasmonic−Photonic Coupling. As mentioned at the beginning, one of the interesting properties of ITO plasmonics is that the plasma frequency is tunable. Photonic modes result from the geometric arrangement of nanorods, while the LSPR is intrinsic to an individual nanorod; thus we expect that a variation of the plasma frequency will affect LSPR strongly, while the photonic resonance should be less sensitive. However, when these two modes overlap, the line shape will vary as a function of the relative position of LSPR and photonic modes, creating a Fano-type line shape. To illustrate the interaction of the plasmon resonance and the lattice resonance, the 5 μm tall ITO-NRA of the square lattice was annealed in air to reduce the plasma frequency by reducing the number of charge carriers contributed from oxygen vacancies (Figure 8).[33] Compared to the as-synthesized sample, it was found that the broad dip shifted to longer wavelength with longer annealing time (indicated by the black arrow), which is consistent with a reduction of the transverse LSPR frequency owing to the

dx.doi.org/10.1021/ph400038g | ACS Photonics 2014, 1, 163−172

reduction of the plasma frequency (eq 1). On the other hand, the dips marked with a black dashed line remain at the same wavelength as the broad LSPR feature traverses across it, albeit with some modification of the line shape.[47] Another notable trend is that the second-order photonic resonance feature at around 1.1 μm (marked with a blue dashed line) is enhnaced with annealing. This is probably due to the increase in dielectric contrast between ITO and air at that wavelength associated with the decrease of the plasma frequency. It was also found that the shift of plasmon resonance ceased with longer annealing time.

In order to elucidate the nature of the photonic modes, from which we can identify the possible energy dissipation channels, the backscattering for the 3 min annealed sample was measured and is shown as the green dashed curve in Figure 8a. The backscattering intensity peaks at the two photonic resonances, and they coincide with the two photonic resonance positions in specular reflectance. We then proceeded with FEM simulation to plot the specular reflectance, absorption, and the intensity of relevant diffraction orders [−1 0] and [−2 0]. The simulated specular reflectance matches well with our experimental measurement, and the calculated diffraction orders match with our backscattering measurement, as shown in Figure 8b. There is a side peak located at the shorter wavelength side of the main peak at 2.35 μm, which does not appear in our experimental result. This is because the diffraction angle of this side peak deviates from the acceptance angle of our optical detector. The other diffraction orders were also calculated, and the intensities of those are negligible, which indicates that the strong backscattering from the two diffraction orders is the result of the photonic stop band at the Brillouin zone edge.[26,48]

The result of the plasmonic−photonic coupling is a creation of absorption minimum, which is clearly shown in Figure 8b. Interestingly, the absorption minimum is located on the shorter wavelength side of the position where the backscattering is strongest, and this decrease of absorption was the reason for the peak located at the same spectral position in the specular reflectance curve, implying an electromagnetically induced transparency.[49,50]

Another interesting observation from Figure 8a is that the line shape at the vicinity of the [−1 0] resonance does not change much when the LSPR traverses across it, except when it is at the high-energy edge of the broad LSPR peak. We attribute this to the relative intensity change between the LSPR and photonic mode being quite small to affect the interaction as the LSPR traverses across the photonic mode, and the line shape remains the same unless the photonic mode is at the edge of the LSPR peak, where the LSPR intensity starts to decrease sharply.

Figure 9a shows the s-wave reflectance spectra for three sets of samples with different heights measured for φ = 0 and θ = 76°. All of these show sharp oscillatory features between 2.1 and 2.4 μm. The strength of the features increases with the height. The FEM simulations fit reasonably well with the reflectance spectra as shown in Figure 9b. The oscillations caused by the interaction of the photonic mode and the transverse LSPR mode are stronger in the simulations; however, the locally created reflectance maxima due to the interaction are obvious for all cases. The weaker interaction signals in the experiments are likely due to the angular variance of the measurement setup and the fact that in the arrays there are small numbers of defects, such as missing or displaced rods, which will decrease the strength of the photonic resonances.

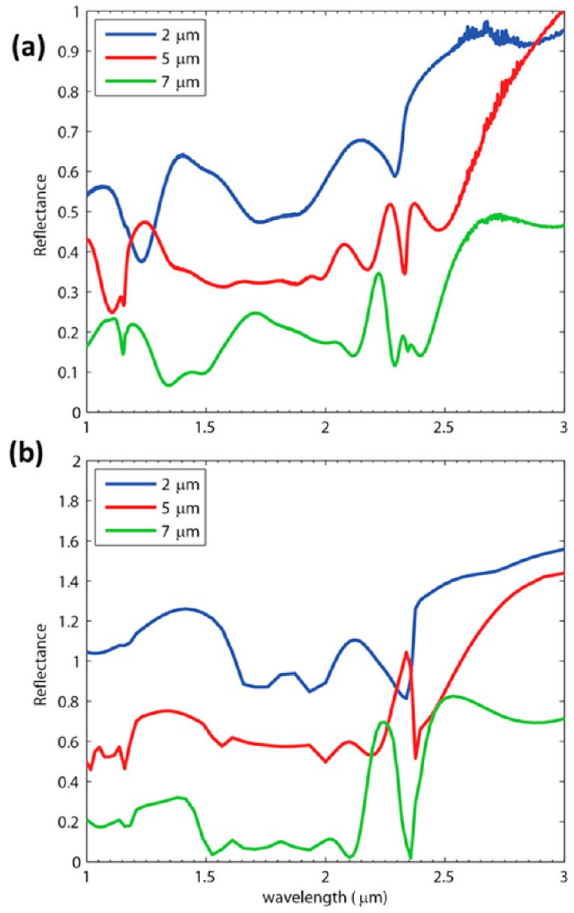

Figure 9. (a) Reflectance curves of square lattice NRAs with three different heights. (b) Reflectance curves from the FEM simulation.

As mentioned above, at high polar angles, the specular reflectances of ITO-NRA are very sensitive to the polarization; only s-polarized light excites strong transverse LSPR due to its in-plane electric field. This property can be exploited to turn on and off the plasmonic−photonic interaction. As shown in Figure 10, the solid blue curve is the reflectance spectrum with p-polarized light; note the [−1 0] photonic mode is sharper with less oscillations compared with that from s-polarized light (shown as a solid red curve), due to minimal interference from transverse LSPR.

Another interesting property of the ITO-NRA system is that by rotating the azimuthal angle, the interference can also be turned off. In Figure 10, the specular reflectances measured at φ = 0° and 45° clearly show that the [−1 0] photonic mode disappears at φ = 45°, while a new photonic mode [−1 1] appears at a different wavelength. This tunability through polarization and azimuthal rotations has many potential applications, such as pulse shaping, nonlinear optical switching based on gap solitons,[51,52] and optical communication.[53]

CONCLUSION

We have carried out a systematic study of light scattering from ITO nanorods in the near-infrared, starting with a simple theoretical analysis for the case of isolated ITO nanorods, followed by 3-D simulations for an array of these nanorods. Our special focus has been on the effects of coupling between transverse plasmonic and photonic modes in these 2-D periodic ITO-NRAs. Using simulations, we were able to design and

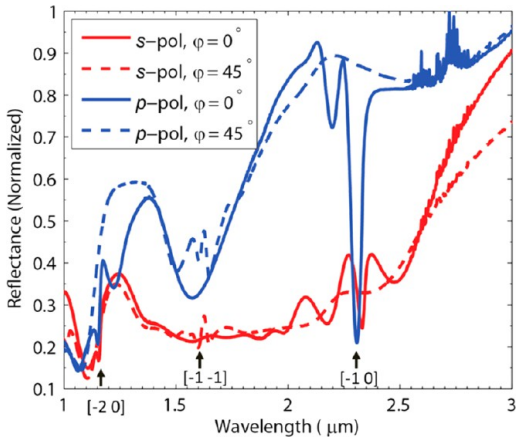

Figure 10. Specular reflectance curves of 5 μm tall square lattice ITO-NRA at a fixed polar angle (θ = 76°). Measurements were performed for two different polarizations (blue curves are p-polarized and red curves are s-polarized) and two high-symmetry azimuthal angles (solid curves: φ = 0°, dashed curves: φ = 45°). Black arrows indicate the position of the photonic modes observed.

interpret a set of experiments where strong mode couplings were observed. The experimental observations agreed well with the simulations at the far field, and the near-field simulation results provide us with the details of the interactions of LSPRs with the photonic resonances. Due to the unique properties of ITO, we are able to tune the plasma frequency through a postgrowth annealing process. Using this tuning capability, we demonstrated experimentally a shift of the resonant coupling that is solely due to the shift of LSPR. With the high aspect ratios of our ITO nanorods and two-dimensional lattice, we have demonstrated that the strength of the mode coupling can be varied through the polarization and the angle of the incident light. The versatile property of the ITO-NRA studied here can potentially be utilized for applications such as infrared sensing, switching, and optical communication.

■ ASSOCIATED CONTENT

Supporting Information

The application of Mie theory to our nanorod system, the FEM simulation setup, additional experiments and simulations that we cited in the text, and how the reflectance spectra were calculated are included in the Supporting Information. This information is available free of charge via the Internet at http://pubs.acs.org.

■ AUTHOR INFORMATION

Corresponding Author

*E-mail: r-chang@northwestern.edu.

Author Contributions

S.Q.L. and R.P.H.C. designed the research. W.Z., Y.H., L.E.O., and S.Q.L. performed gold array patterning. D.B.B. performed ITO film growth. S.Q.L. performed the optical measurements and array growth. P.G. implemented the FEM model and performed the FEM simulation. S.Q.L. performed the single-rod analysis, DDA simulation, and part of the FEM simulation (Figure 8b). All authors contributed to the data analysis, figure preparation, and manuscript writing.

Notes

The authors declare no competing financial interest.

■ ACKNOWLEDGMENTS

This would not have been possible without the support of NSF funding (DMR-1121262 and DMR 0843962), QUEST computational resources (Project p20194 and Project p20447), and Center for Nanoscale Materials in Argonne National Laboratory (Project CNM 25883 and Project CNM 30831). Various characterizations were done at the NUANCE Center and KECK II Facilities at Northwestern University. The NUANCE Center and KECK II Facilities are supported by the NSF-NSEC, NSF-MRSEC, Keck Foundation, the State of Illinois, and Northwestern University. Discussions with Dr. Piotr Flatau and Dr. Bruce Draine on DDA simulation methods and discussions with Dr. Pierfrancesco Zilio and Dr. Lynn An on COMSOL FEM simulations have accelerated the production of this work significantly. e-Beam lithography was performed with a JEOL-9300 at the Center for Nanoscale Materials at Argonne National Laboratory. Use of the Center for Nanoscale Materials was supported by the U.S. Department of Energy, Office of Science, Office of Basic Energy Sciences, under Contract No. DE-AC02-06CH11357.

■ REFERENCES

(1) Wei, H.; Wang, Z.; Tian, X.; Käll, M.; Xu, H. Cascaded logic gates in nanophotonic plasmon networks. *Nat. Commun.* **2011**, *2*, 387.
(2) Lukin, M. Colloquium: Trapping and manipulating photon states in atomic ensembles. *Rev. Mod. Phys.* **2003**, *75*, 457.
(3) Anker, J. N.; Hall, W. P.; Lyandres, O.; Shah, N. C.; Zhao, J.; Van Duyne, R. P. Biosensing with plasmonic nanosensors. *Nat. Mater.* **2008**, *7*, 442−53.
(4) Berini, P.; De Leon, I. Surface plasmon-polariton amplifiers and lasers. *Nat. Photonics* **2011**, *6*, 16−24.
(5) Zhou, W.; Dridi, M.; Suh, J. Y.; Kim, C. H.; Wasielewski, M. R.; Schatz, G. C.; Odom, T. W. Lasing action in strongly coupled plasmonic nanocavity arrays. *Nat. Nanotechnol.* **2013**, *8*, 506−511.
(6) Engheta, N. Circuits with light at nanoscales: optical nanocircuits inspired by metamaterials. *Science* **2007**, *317*, 1698−1702.
(7) Ozbay, E. Plasmonics: merging photonics and electronics at nanoscale dimensions. *Science* **2006**, *311*, 189−193.
(8) Sorger, V. J.; Oulton, R. F.; Ma, R.-M.; Zhang, X. Toward integrated plasmonic circuits. *MRS Bull.* **2012**, *37*, 728−738.
(9) Auguié, B.; Barnes, W. L. Collective resonances in gold nanoparticle arrays. *Phys. Rev. Lett.* **2008**, *101*, 143902.
(10) Zhou, W.; Odom, T. W. Tunable subradiant lattice plasmons by out-of-plane dipolar interactions. *Nat. Nanotechnol.* **2011**, *6*, 423−427.
(11) Carron, K. T.; Fluhr, W.; Meier, M.; Wokaun, A.; Lehmann, H. W. Resonances of two-dimensional particle gratings in surface-enhanced raman scattering. *J. Opt. Soc. Am. B* **1986**, *3*, 430−440.
(12) Aizpurua, J.; Bryant, G. W.; Richter, L. J.; De Abajo, F. J. G.; Kelley, B. K.; Mallouk, T. Optical properties of coupled metallic nanorods for field-enhanced spectroscopy. *Phys. Rev. B* **2005**, *71*, 235420.
(13) Draine, B. T.; Flatau, P. J. Discrete-dipole approximation for periodic targets: theory and tests. *J. Opt. Soc. Am. A* **2008**, *25*, 2693−2703.
(14) Laroche, M.; Albaladejo, S.; Carminati, R.; Sáenz, J. J. Optical resonances in one-dimensional dielectric nanorod arrays: field-induced fluorescence enhancement. *Opt. Lett.* **2007**, *32*, 2762−2764.
(15) Rodriguez, S. R. K.; Abass, A.; Maes, B.; Janssen, O. T. A.; Vecchi, G.; Gómez Rivas, J. Coupling bright and dark plasmonic lattice resonances. *Phys. Rev. X* **2011**, *1*, 021019.
(16) Zou, S.; Schatz, G. C. Silver nanoparticle array structures that produce giant enhancements in electromagnetic fields. *Chem. Phys. Lett.* **2005**, *403*, 62−67.
(17) Zou, S.; Janel, N.; Schatz, G. C. Silver nanoparticle array structures that produce remarkably narrow plasmon lineshapes. *J. Chem. Phys.* **2004**, *120*, 10871−10875.

(18) Vecchi, G.; Giannini, V.; Gómez Rivas, J. Shaping the fluorescent emission by lattice resonances in plasmonic crystals of nanoantennas. *Phys. Rev. Lett.* **2009**, *102*, 146807.
(19) Natarov, D. M.; Byelobrov, V. O.; Sauleau, R.; Benson, T. M.; Nosich, A. I. Periodicity-induced effects in the scattering and absorption of light by infinite and finite gratings of circular silver nanowires. *Opt. Express* **2011**, *19*, 22176−22190.
(20) Ghenuche, P.; Vincent, G.; Laroche, M.; Bardou, N.; Haïdar, R.; Pelouard, J.-L.; Collin, S. Optical extinction in a single layer of nanorods. *Phys. Rev. Lett.* **2012**, *109*, 143903.
(21) Hibbins, A. P.; Evans, B. R.; Sambles, J. R. Experimental verification of designer surface plasmons. *Science* **2005**, *308*, 670−672.
(22) Byelobrov, V. O.; Ctyroky, J.; Benson, T. M.; Sauleau, R.; Altintas, A.; Nosich, A. I. Low-threshold lasing eigenmodes of an infinite periodic chain of quantum wires. *Opt. Lett.* **2010**, *35*, 3634−3636.
(23) Li, Z.-Y.; Gu, B.-Y.; Yang, G.-Z. Large absolute band gap in 2d anisotropic photonic crystals. *Phys. Rev. Lett.* **1998**, *81*, 2574.
(24) Kempa, K.; Kimball, B.; Rybczynski, J.; Huang, Z.; Wu, P.; Steeves, D.; Sennett, M.; Giersig, M.; Rao, D.; Carnahan, D. Photonic crystals based on periodic arrays of aligned carbon nanotubes. *Nano Lett.* **2003**, *3*, 13−18.
(25) Joannopoulos, J. D.; Johnson, S. G.; Winn, J. N.; Meade, R. D. *Photonic Crystals: Molding the Flow of Light*; Princeton University Press, 2011.
(26) Sakoda, K. *Optical Properties of Photonic Crystals*; Springer: Berlin, 2005; Vol. *80*.
(27) Marquier, F.; Arnold, C.; Laroche, M.; Greffet, J. J.; Chen, Y. Degree of polarization of thermal light emitted by gratings supporting surface waves. *Opt. Express* **2008**, *16*, 5305−5313.
(28) Yao, J.; Liu, Z.; Liu, Y.; Wang, Y.; Sun, C.; Bartal, G.; Stacy, A. M.; Zhang, X. Optical negative refraction in bulk metamaterials of nanowires. *Science* **2008**, *321*, 930.
(29) Liu, Y.; Bartal, G.; Zhang, X. All-angle negative refraction and imaging in a bulk medium made of metallic nanowires in the visible region. *Opt. Express* **2008**, *16*, 15439−15448.
(30) Wurtz, G. A.; Pollard, R.; Hendren, W.; Wiederrecht, G. P.; Gosztola, D. J.; Podolskiy, V. A.; Zayats, A. V. Designed ultrafast optical nonlinearity in a plasmonic nanorod metamaterial enhanced by nonlocality. *Nat. Nanotechnol.* **2011**, *6*, 107−111.
(31) Kabashin, A. V.; Evans, P.; Pastkovsky, S.; Hendren, W.; Wurtz, G. A.; Atkinson, R.; Pollard, R.; Podolskiy, V. A.; Zayats, A. V. Plasmonic nanorod metamaterials for biosensing. *Nat. Mater.* **2009**, *8*, 867−71.
(32) Lyvers, D. P.; Moon, J.-M.; Kildishev, A. V.; Shalaev, V. M.; Wei, A. Gold nanorod arrays as plasmonic cavity resonators. *ACS Nano* **2008**, *2*, 2569−2576.
(33) Li, S. Q.; Guo, P.; Zhang, L.; Zhou, W.; Odom, T. W.; Seideman, T.; Ketterson, J. B.; Chang, R. P. H. Infrared plasmonics with indium−tin-oxide nanorod arrays. *ACS Nano* **2011**, *5*, 9161−9170.
(34) Payne, E. K.; Shuford, K. L.; Park, S.; Schatz, G. C.; Mirkin, C. A. Multipole plasmon resonances in gold nanorods. *J. Phys. Chem. B* **2006**, *110*, 2150−2154.
(35) Mie, G. Beiträge zur optik trüber medien, speziell kolloidaler metallösungen. *Ann. Phys.* **1908**, *330*, 377−445.
(36) Novotny, L. Effective wavelength scaling for optical antennas. *Phys. Rev. Lett.* **2007**, *98*, 266802.
(37) Bohren, C. F.; Huffman, D. R., *Absorption and Scattering of Light by Small Particles*; Wiley & Sons: Weinheim, Germany, 1983; p 530.
(38) Granqvist, C. G.; Hultaker, A. Transparent and conducting ito films: new developments and applications. *Thin Solid Films* **2002**, *411*, 1−5.
(39) Draine, B. T.; Flatau, P. J. Discrete-dipole approximation for scattering calculations. *J. Opt. Soc. Am. A* **1994**, *11*, 1491−1491.
(40) Flatau, P.; Draine, B. Fast near field calculations in the discrete dipole approximation for regular rectilinear grids. *Opt. Express* **2012**, *20*, 1247−1252.
(41) Christ, A.; Tikhodeev, S.; Gippius, N.; Kuhl, J.; Giessen, H. Waveguide-plasmon polaritons: strong coupling of photonic and electronic resonances in a metallic photonic crystal slab. *Phys. Rev. Lett.* **2003**, *91*, 183901.
(42) Barnes, W. L.; Dereux, A.; Ebbesen, T. W. Surface plasmon subwavelength optics. *Nature* **2003**, *424*, 824−830.
(43) Zhang, S.; Genov, D. A.; Wang, Y.; Liu, M.; Zhang, X. Plasmon-induced transparency in metamaterials. *Phys. Rev. Lett.* **2008**, *101*, 047401.
(44) Rodriguez, S. R. K.; Janssen, O. T. A.; Lozano, G.; Omari, A.; Hens, Z.; Rivas, J. G. Near-field resonance at far-field-induced transparency in diffractive arrays of plasmonic nanorods. *Opt. Lett.* **2013**, *38*, 1238−1240.
(45) Wan, Q.; Feng, P.; Wang, T. H. Vertically aligned tin-doped indium oxide nanowire arrays: Epitaxial growth and electron field emission properties. *Appl. Phys. Lett.* **2006**, *89*, 123102.
(46) Henzie, J.; Lee, M. H.; Odom, T. W. Multiscale patterning of plasmonic metamaterials. *Nat. Nanotechnol.* **2007**, *2*, 549−554.
(47) Fano, U. Effects of configuration interaction on intensities and phase shifts. *Phys. Rev.* **1961**, *124*, 1866−1878.
(48) Tikhodeev, S. G.; Yablonskii, A.; Muljarov, E.; Gippius, N.; Ishihara, T. Quasiguided modes and optical properties of photonic crystal slabs. *Phys. Rev. B* **2002**, *66*, 045102.
(49) Taubert, R.; Hentschel, M.; Giessen, H. Plasmonic analog of electromagnetically induced absorption: simulations, experiments, and coupled oscillator analysis. *J. Opt. Soc. Am. B* **2013**, *30*, 3123−3134.
(50) Zhang, S.; Genov, D. A.; Wang, Y.; Liu, M.; Zhang, X. Plasmon-induced transparency in metamaterials. *Phys. Rev. Lett.* **2008**, *101*, 47401.
(51) Eggleton, B. J.; Slusher, R.; de Sterke, C. M.; Krug, P. A.; Sipe, J. Bragg grating solitons. *Phys. Rev. Lett.* **1996**, *76*, 1627.
(52) Aceves, A. B. Optical gap solitons: past, present, and future; theory and experiments. *Chaos* **2000**, *10*, 584−589.
(53) Bogaerts, W.; Taillaert, D.; Dumon, P.; Van Thourhout, D.; Baets, R. A polarization-diversity wavelength duplexer circuit in silicon-on-insulator photonic wires. *Opt. Express* **2007**, *15*, 1567−1578.